Chapter 3

Optical, Mechanical, and Chemical Properties of Na_2O-P_2O_5-SiO_2-based Tint Glass for Building Construction Applications

3.1 Introduction

Over the past few years, multistorey buildings worldwide have made substantial use of structural glass and glass ceramics as their primary envelope material. Undoubtedly, the importance is growing daily, and contemporary glass research in particular regions-such as Saudi Arabia, the United Arab Emirates, India, and others- focuses on optimizing optical qualities including transmittance, absorbance, and reflectance. If extremely clear pure silica glasses are used as envelopes, the structures will be subjected to extreme cooling loads and uncomfortable conditions. This was beneficial for optimizing daylighting, but this restriction has been overcome using clear tint glasses, that partially prevent solar radiations that heat buildings. These glasses are created, usually, by incorporating metal oxides, including iron, tin, copper, manganese, chromium, vanadium, etc., into the molten glass. In addition, metal coatings, such as gold, silver, copper, and aluminum, are placed on the glass's surface to enhance heat and light reflections. where a few noteworthy studies and methods on reflective layers have been carried out to create single and multi-layer metal coatings, such as zinc sulfide anti-reflection layers with a subsequent metal layer of high infrared reflection capacity, such as gold, silver, or copper, to create heat-reflective glass using the vacuum deposition technique [4]. A thin heat-reflecting layer is made up of one or more metal oxides, including the oxides of heavy metals like Co, Cr, Ni, Fe, Sn, Mn, and Ti, which are created by the thermal decomposition of appropriate compounds of the corresponding metals on the glass surface [5]. A thin layer of silicon oxide comes next by the vacuum deposition of titanium injected on top of the silicon oxide layer after the method of oxidization at temperatures above 550˚C to generate titanium oxide in the rutile phase [39]. A metal Zn film is deposited on top of

an Ag or Cu heat-reflective film that has been deposited on top of an ITO or AIN film that has been applied to the outermost layer of the glass surface, etc. [40]. At the same time, more research has been done to create low-emissivity building envelopes through the production of various low-E glass types. Hollow low-E glasses for office building windows have been developed to improve annual energy savings, and in some instances, the assessment of the spectral characteristics of clear, double, and triple low-E glasses has led to the development of an efficient energy glass model for solar radiation in the buildings [6,41]. In addition to emissivity and reflection, several academic studies have been conducted to regulate the amount of sunlight that enters office buildings. These studies have used double-glazed windows with highly reflective blinds and variable blind tilt angles to allow daylighting to pass through as needed. A numerical simulation approach for this study has also been established [7]. However, in reading room structures in India's hot and dry climate zone, many kinds of external shading systems on bronze glass windows have been tested to determine the ideal heat gain and daylighting [42]. By examining the heat transmission via an interior louvered blind constructed of double-glazed glasses, the thermal transmittance was ascertained and additionally, a biquadratic equation was created at different points compared with computational fluid dynamics [43]. The thermal performance of residential buildings with and without windows, as well as those with integrated adaptive kinetic shading systems, was previously investigated by earlier researchers [44]. A suitable percentage of dissatisfaction (PPD) was estimated in an intriguing study using data from the examination of 1280 glass windows with film, 45 different types of films, and connections for choosing a suitable glass window with film to serve as a building envelope in buildings situated in hot environments and thermal comfort of the inhabitants seated close to the glass window [45]. Light- and heat-absorbing pigmented glasses made by fusing Se, CoO, FeO, and Fe_2O are another highly effective method

used by the researchers to attain the ideal degree of thermal comfort; UV data and other features of these LHA glasses were collected and published [46]. To minimize heat gain in buildings in hot and arid zones consisting of India, double float, float, and tinted glasses are usually employed professionally [47]. At some times, heat acquisition information for buildings with float and tinted glass windows during the summer for all eight coordinate directions of Indian climatic regions was examined and presented [48]. Simultaneously experimental analyses of the visible characteristics of various tinted and reflecting window glass types lead to the improvement of the daylight factor in buildings located in warm, humid climates such as India [49]. Numerous prior studies have examined various glass compositions using XRD, FTIR, and UV-Visible spectroscopy. Based on these characterizations, the researchers have inferred physical and significant optical parameters, including molar refraction, optical band gap, Urbach energy, dielectric constant, and metallization parameter [8, 9, 33, 50]. In addition, since tint glasses serve as envelope material, it is crucial to investigate their mechanical properties, such as their compressive strength. In associated research, bulk metallic glasses made of magnesium, copper, zinc, and yttrium oxide (Mg-Cu-Zn-Y) having elevated compressive strengths were examined due to their inexpensiveness, lightweight, and growing popularity [10]. In further research assessing Weibull statistics and the compositional dependence on malleability, an investigation on the compressive strength of Cu-Hf-Al bulk metallic glasses was recently reported [51]. Another study reveals that an assortment of quaternary Fe-B-Si-Zr bulk metallic glasses injected with a high concentration of Fe produced tinted glass with exceptionally high compressive strength and good soft magnetic characteristics [11]. The aforementioned literature surveys demonstrate the important roles that Fe, Cu, B, Zr, and Mg play in enhancing the mechanical properties of glasses. Inspired by these studies, the work being discussed now focuses on creating a novel structure based on Fe and Cu that produces a blue-

colored, pigmented stannic soda phosphate silicate glass structure while assessing its optical, physical, and mechanical properties. This work will be helpful in the creation of solar passive building envelopes that are energy efficient.

3.2 Experimental details

3.2.1 *Preparation of tint glass samples*

To create the experimental sample for the referred iron and copper-based stannic soda phosphate silicate tint glass system ($0.2Cu_2O$-$0.07CuO$-$0.03Fe_2O_3$-$0.3SnO_2$)-$0.4P_2O_5$-$30Na_2O$-$69SiO_2$was synthesized, and the using calibrated mixture of chemical ingredients in the weight proportion is specified in **Table 3.1**. Wherein iron oxide (Fe_2O_3, 98% purity), tin oxide (SnO_2, 98% purity), ammonium dihydrogen orthophosphate ($(NH_4)H_2PO_4$, 97% purity), sodium carbonate (Na_2CO_3, 99% purity), and quartz (SiO_2, 99% purity) supplied by Lobachemie have been used as sources of Fe_2O_3, SnO_2, P_2O_5, Na_2O, and SiO_2, respectively. In which cuprous oxide (Cu_2O, 97% purity) and cupric oxide (CuO, 97% purity) provided by Avarice industries were utilized as sources of Cu_2O and CuO, respectively. To prepare the evaluated substances for melting in an electric furnace heated by SiC rod, the weight of each component was measured accurately using an electronic microanalytical balancing machine. The determined time-temperature profile and ramping rate of the melting procedure are also displayed in **Fig. 3.1(a)**. To create more homogenous glass structures, the melted glasses were then put over a heated alumina plate, cooled, crushed, and remelted at the temperature profile that had been set earlier. The remelted glasses then flowed once more onto heated iron molds with specified sizes. The annealing with a predetermined time-temperature profile, ramping, and cooling at the rates indicated in **Fig. 3.1(b)** came next. The samples were labeled as indicated in **Table 3.2** for optical and mechanical evaluation after being mechanically cut to shape using a glass cutter and polished with silicon carbide (SiC) and cerium

oxide (CeO_2). **Fig. 3.2** displays an image of the optically polished rectangular glass samples that were ready for optical characterization.

Table 3.1. This table lists the elements' chemical makeup in the original glass batch composition.

Ingredient	Wt. (gram)	Estimated chemical concentration (Wt. %)
Cuprous oxide (Cu_2O)	**0.3**	**0.4**
Cupric oxide (CuO)	**0.05**	**0.07**
Iron oxide (Fe_2O_3)	**0.05**	**0.07**
Tin oxide (SnO_2)	**0.5**	**0.7**
ammonium dihydrogen orthophosphate ($(NH_4)H_2PO_4$)	**1**	**1.3**
Sodium carbonate (Na_2CO_3)	**32**	**42.1**
Quartz (SiO_2)	**42**	**55.26**

3.2.2 *XRD measurement*

The generated compositions' X-ray diffraction scans (XRD) were recorded to support the amorphous nature of the samples employing a Ragaku Smart Lab (9KW) powder-type XRD machine from RIGAKU Corporation company (Japan) equipped with a graphite monochromatized copper Kα radiation source (λ=1.540) and Ni filter tube functioned at 40 kV and 20 mA current with an angular value (2θ) of 10-80º at a scan rate of 3º min^{-1} at ambient temperature at all the particular stages, such as before melting, before and after heat treatments, where derived sets of data were examined applying PANalytical XPert High Score in addition matching with standard ICDD (International Centre for Diffraction Data) cards.

Table 3.2. This table shows the density and dimensions of all the prepared tinted glass samples.

Sample	Depth	Width	Length				Density(ρ)

	(mm)	(mm)	(mm)	Dry weight (W_d) (gram)	Soaked weight (W_W) (gram)	Suspended weight (W_s) (gram)	($\frac{W_d \times \rho_{water}}{W_W - W_s}$) (gram/cm^3)
u/1	**4.00**	**14.31**	**21.52**	**2.26**	**2.28**	**1.35**	**2.43**
u/2	**4.20**	**18.66**	**21.81**	**2.57**	**2.59**	**1.52**	**2.40**
u/3	**4.80**	**12.90**	**19.63**	**3.25**	**3.27**	**1.94**	**2.45**
u/4	**6.90**	**14.91**	**23.47**	**5.34**	**5.36**	**3.18**	**2.46**
A/1	**12.07**	**7.00**	**7.00**	**1.26**	**1.27**	**0.75**	**2.43**
A/2	**12.46**	**8.00**	**8.00**	**1.74**	**1.74**	**1.04**	**2.47**
A/3	**12.88**	**8.50**	**8.50**	**1.96**	**1.96**	**1.17**	**2.47**
A/4	**13.62**	**17.89**	**26.43**	**14.37**	**14.34**	**8.57**	**2.49**
A/5	**16.23**	**19.93**	**24.65**	**16.31**	**16.33**	**9.73**	**2.47**
A/6	**17.95**	**20.27**	**21.44**	**17.20**	**17.23**	**10.24**	**2.46**

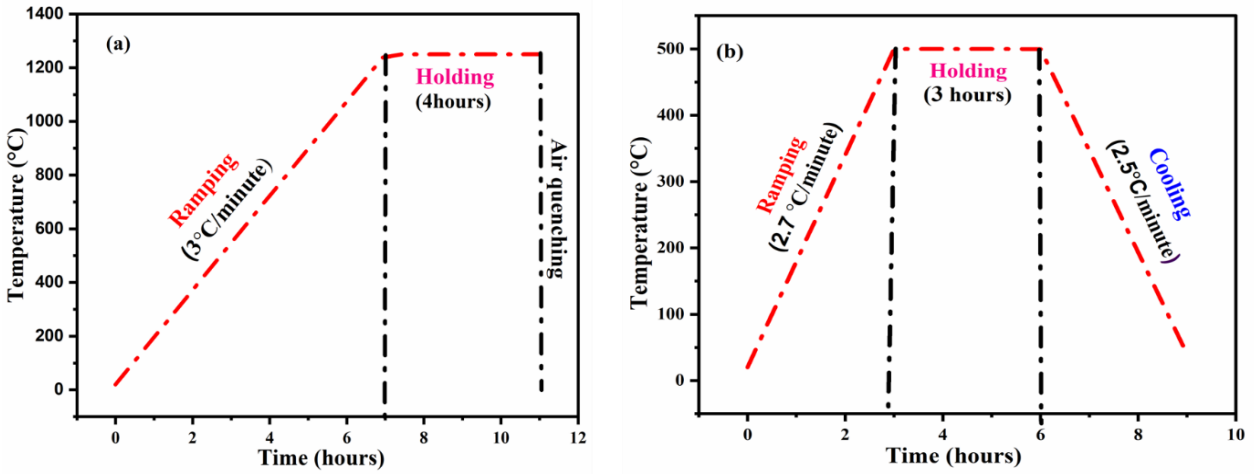

Fig. 3.1 This figure shows the time-temperature profiles for the melt-quench process (a) and the annealing process (b).

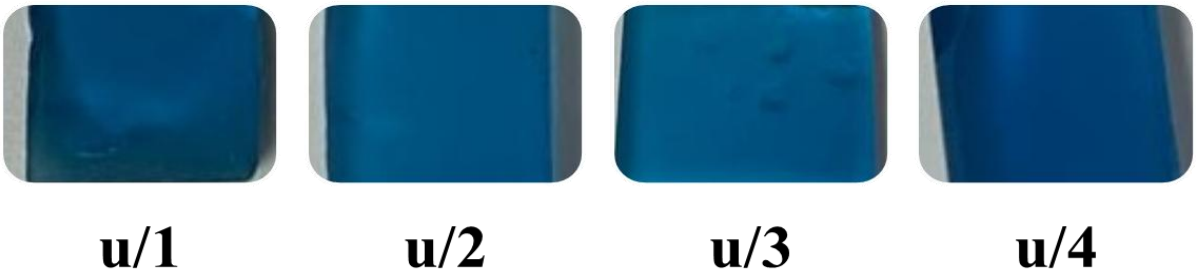

Fig. 3.2. Photographs of the optically characterized, polished glass samples are shown, where sample u/1 has dimensions of 21.52 mm in length, 14.31 mm in breadth, and 4.00 mm in thickness; sample u/2 measures 21.81 mm in length, 18.66 mm in breadth, and 4.20 mm in thickness; sample u/3 has dimensions of 19.63 mm in length, 12.90 mm in breadth, and 4.80 mm in thickness; and sample u/4 measures 23.47 mm in length, 14.91 mm in breadth, and 6.90 mm in thickness.

3.2.3 *FTIR spectroscopy measurement*

To identify the functional groups in the samples, the amount of the mentioned developed glass powder blended with potassium bromide in 1:100 ratios and then pressed under 6 tons/cm^2 pressure in a mold for 120 seconds to create pallet discs was established. The respected pallet discs were then immediately assessed with a Nicolet iS5 FTIR Fourier transform infrared spectrometer from THERMO Electron Scientific Instruments LLC company (USA) at a resolution of 4 cm^{-1}, within the 450–4000 cm^{-1} range, in the transmittance mode at ambient temperature to prevent moisture attacks on the specimens.

3.2.4 *UV-VIS spectroscopy measurement*

Using a Jasco V-770 double beam UV-VIS spectrophotometer (Japan) connected to a PC running UV-Win lab software, the ultraviolet and visible (UV) spectra of optically polished glass samples (u/1, u/2, u/3, and u/4) (**Fig. 3.2**) of dimensions specified in **Table 3.2** and etched by silicon carbide (SiC) and cerium oxide (CeO_2) were captured. When measuring the visible and solar optical properties of the tint glass samples, the weighted average of the experimental data collected using

the normal incidence of light in the entire visible spectral which encompasses transmission in the specular transmission mode, reflection in the diffuse reflection mode, and absorption in the spectrum mode-between 360 and 830 nm in wavelength was used. A US standard atmosphere containing 3.4 mm of ozone and 20 mm of precipitable H_2O vapor, typically in a very clear atmosphere, was utilized to collect weighted factors for calculating solar optical characteristics [37].

3.2.5 *Physico-mechanical properties measurement*

The density of the glass bar samples with the dimensions listed in **Table 3.2** was determined at the ambient temperature applying the Archimedes principle and water as the immersion medium. The glass bars were heated in water to a temperature of more than 100 °C for two hours through an electric heater to obtain the shocked weights of the samples.

Furthermore, three glass bar samples (A/1, A/2, and A/3) were selected for mechanical testing. The mentioned samples were then formed by cutting a water-cooled low-speed diamond saw into the proper sizes based on the ASTM D695 standards protocol. Then the bars' edges were repeatedly filed and polished using 400/800/1200 water-cooled SiC grits and 6/3/1/.025 µm diamond pastes ensuring that both edges are adjacent to each other with a deviation of no more than.05 cm. The samples were then thoroughly rinsed in water, dried using a warm air blower, and re-annealed with the precise time-temperature profile, ramping, and cooling rate illustrated in **Fig. 3.1(b)** to eliminate any residual stresses created when cutting, grinding, and polishing. The samples' lack of residual stresses was further confirmed by employing a polariscope and, the mechanical properties of these three samples were then evaluated by employing a Tinius Olsen H10KL universal tensile machine (UTM) featuring a prearranged setup.05 mm/min crosshead speed under 10 MN load cell.

The stress-strain diagram was used for calculating the young modulus using the following equation.

$$\sigma_C = \frac{P}{A}$$

$$\varepsilon = \frac{D}{d}$$

$$E = \frac{\sigma_C}{\varepsilon}$$

In this case, σ_C stands for compressive strength, P for the load (Newton), A for the surface area of load (mm^2), ε for compressive strain, D for displacement measured by the instrument along the sample thickness prior to failure, d for sample thickness, and E for the young module.

3.2.6 *Chemical durability measurement*

After the initial weight measurements of the three glass bar samples (A/1, A/4, and A/6) with dimensions given in **Table 3.2** for assessing chemical durability, which is an indicator of their ability to resist chemical attacks [**38**], the specimens' weight loss in a corrosive environment was evaluated. This was done by placing the respective samples in a fixed concentration of 1 (N) of HNO_3, H_2SO_4, and HCl for a week at ~ 25 °C. Then, the weight loss of the respective samples was measured, and the corresponding chemical durability parameters were also computed using the equation described below.

$$\text{Chemical durability (gram/ (cm}^2\text{. hour)} = \frac{W_i - W_f}{st}$$

In which s is the glass piece's surface area, t is the time, and W_i = Initial weight of the glass bar samples (A/1, A/4, and A/6) measured before being immersed in the corresponding corrosive liquid; W_f = Final weight of the glass bar samples (A/1, A/4, and A/6) taken after immersed in the corresponding corrosive liquid.

3.3 Results and discussion

The process of creating an effective absorbing tint glass began, due to the primary focus of the relevant research, with the study and identification of multi-metallic materials doped in glass composition. It was discovered that doping of the listed material produces an entirely black and opaque result when it exceeds its maximum limits (<1.24 wt.% and <.6 mol%) in a phosphorus silicate glass matrix. This information further aided in determining the minimum transparency of the glass system, where transparency begins to show at the composition concentration stated in **Table 3.1**, at which point the combined glass structure gained its most fundamental functional characteristics of transparency in visible light [**52**–**55**]. Before melting, the glass composition's total doped metallic material concentrations (Sn^{4+}, Fe^{3+}, Cu^{2+}, and Cu^{+}) were 1.24 weight percent and 0.6-mole percent. When the tinted glass began to show transparency, the maximum total concentration of metallic doped materials (Sn^{4+}, Fe^{3+}, Cu^{2+}, Cu^{+}) in the initial glass composition was optimized. At that point, small amounts of phosphorus oxide (P_2O_5) and the metallic doped materials (Sn^{4+}, Fe^{3+}, Cu^{2+}, Cu^{+}) in their respective mol (%) composition were incorporated into the sodium silicate glass, substituting SiO_2. A small amount of $P_2O_5$was present in the specimen for two main reasons: first, it was used as a dissolving agent to lower the melting temperature of glasses [**56**–**58**], and second, it polymerized the silicate network structure to raise the glass's chemical stability [**59**–**62**]. Moreover, tin is purposefully added to the composition in question, considering it typically imparts a tint to the silicate glass structure on its own [**27**]. The insertion of a small amount of SnO_2 doping in the initial batch is only done for finning, which is the process of safely eliminating bubbles from melted glass [**63**]. Tin's predominant indolence can be explained by the fact that it is reported to exist in two oxidation states in glass: +2 and +4. In certain instances, it can also be found in pairs, where the oxidation state is notably replaced by +4

under oxidizing conditions [62, 64]. The cation Sn^{4+}, which is [Kr] $4d^{10}$, contains a close shell electronic structure, so it should not naturally color the silicate glass structure [65]. In general, SnO_2 changes the structure and properties of glass structures, improves their physical and optical qualities, and occasionally acts as a network modifier [26,27,66,67]. The results of numerous earlier investigations show that the mechanical hardness and thermal stability of glass structures are significantly increased by the enhanced and modified networks that are obtained by optimal SnO_2 infusion [63]. Numerous other studies attest to the fact that optimal SnO_2 doping in silicate glass structures is highly beneficial for improving the temperature stability and photosensitivity of silica glass optical gratings [68]. In addition, even at very low compositional concentrations, tin increases other properties including density and refractive index. These properties are crucial for certain structural alterations brought on by an increase in the bridging oxygen concentration [27]. Tin oxide appears to generally increase the degree of opacification of the formal opaque layer of the glass ceramic coating, which helps mask the color of the metal substrate. SnO_2 has also been considered as an opacifier in a variety of glass applications [69]. However, because SnO_2 is very constrained in its solubility in silicate melt, minimal tin dioxide causes the glass melt to precipitate as finely dispersed cassiterite crystals [28].

3.3.1 *Analysis of XRD*

The glass structure specimens that were synthesized were subjected to X-ray diffraction (XRD) at three distinct stages of the experiment: initial composition, after melt-quench processing, and after heat treatment to eliminate internal stresses. For each of the three stages, the same kinds of curves (**Fig. 3.3**) were observed, with a predominant initial hump attributed to the base glass, as recommended by earlier studies [70]. Additionally, none of the three graphs showed a significant peak, indicating that the sample was amorphous throughout the experiment and that the other

ingredient oxides (i.e., Fe_2O_3, SnO_2, $(NH_4)H_2PO_4$, Cu_2O, and CuO) were not identified as caused by their trace amounts (**Table 3.1**).

3.3.2 *FTIR Analysis*

The FTIR spectroscopy approach was utilized to evaluate the structural characteristics of the synthesized specimen. **Fig. 3.4** displays the infrared transmission spectra of the colored glass. There are two separate zones in the 500–4000 cm^{-1} range, in regards to the IR spectra.

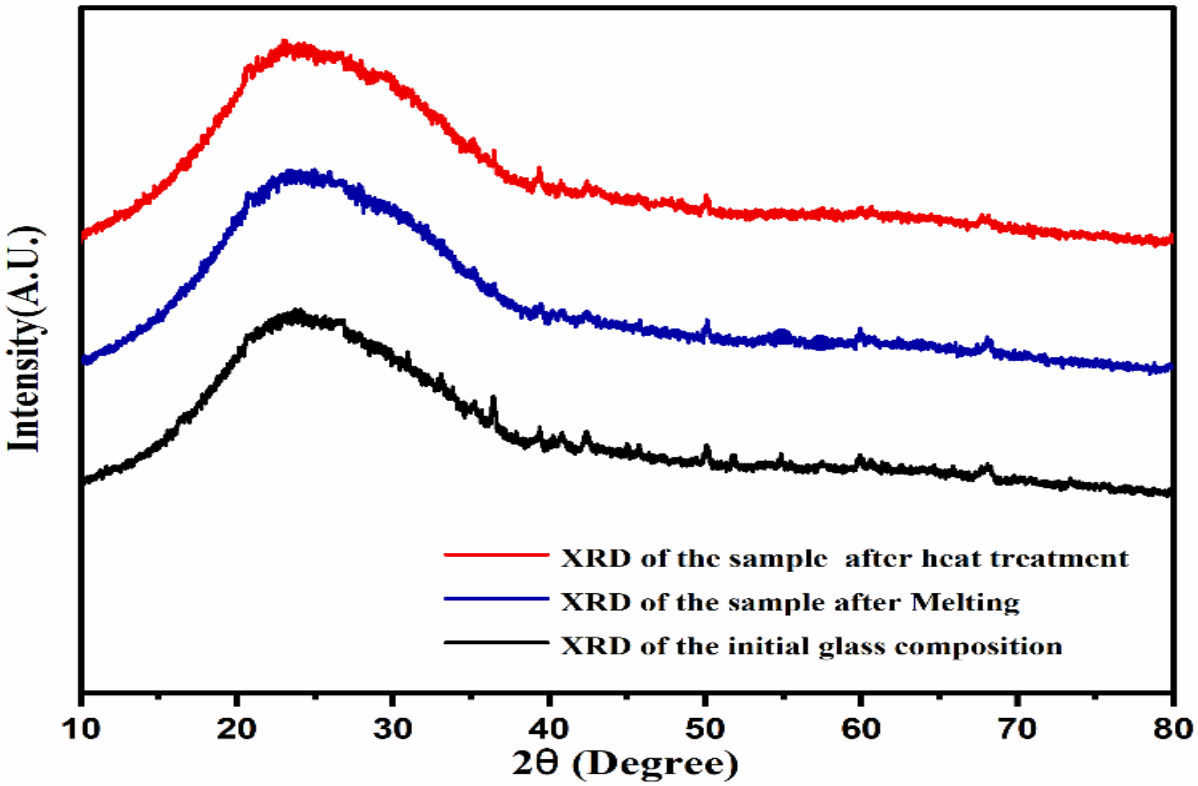

Fig. 3.3. The figure shows the XRD patterns of the initial glass composition, the melted tinted glass powder, and the heat-treated tinted glass.

While the functional group region that emerged in the higher range of the spectrum is crucial to determining the sample's structural details, the distinctive vibrational bands, the majority of which

developed in the lower range of the spectrum, are allocated to the fingerprint region of the infrared spectra. A strong far-infrared broadband was acquired at approximately 1048 cm^{-1}, a very small weak IR band was discovered at approximately 1632 cm^{-1}, a medium-infrared broadband was observed at approximately 3454 cm^{-1}, and a medium-sharp IR band appeared at approximately 455 cm^{-1} and about 765 cm^{-1} (**Fig. 3.4**). The medium broad band at approximately 455 cm^{-1} is caused by the v_4(O-Si-O) bending vibrations in the SiO_4 tetrahedron groups and the broad and strong band acquired around 1048 cm^{-1} was caused by the asymmetric stretching vibration of Si-O (v_3(Si-O)) bond in the SiO4tetrahedron groups that exist in the silicate phases of the glass samples [**70**]. **Table 3.3** provides specifics of the vibration bands and the associated functional groupings. The FTIR spectra verify that the silicate network is unaffected by the total metallic doped concentrations (1.24 wt.% and .6 mol%).

3.3.3 *Spectroscopy of UV-VIS*

The spectral transmission, reflection, and absorbance of the four distinct rectangular glass samples (u/1, u/2, u/3, and u/4) in the visible and ultraviolet wavelength regions are shown in **Fig. 3.5**. The generated pigmented glass's reflection and transparency, as shown in **Figs. 3.5(a)** and **5(b)**, reach their maximum intensity band in the visible spectrum at 480 nm.

3.3.3.1 *Visible Optical Properties*

Using ISO standards, four glass samples' visible characteristics, such as transmittance, reflectance, and absorbance, were measured experimentally[**71**]. The weighted average of the visible optical properties is calculated using the following equations.

$$T_{VIS} = \frac{\sum_{\lambda=360nm}^{\lambda=830nm} D_\lambda \tau(\lambda) v(\lambda) \Delta\lambda}{\sum_{\lambda=360nm}^{\lambda=830nm} D_\lambda v(\lambda) \Delta\lambda}$$

$$R_{VIS} = \frac{\sum_{\lambda=360nm}^{\lambda=830nm} D_\lambda \rho(\lambda) v(\lambda) \Delta\lambda}{\sum_{\lambda=360nm}^{\lambda=830nm} D_\lambda v(\lambda) \Delta\lambda}$$

In this case, $\Delta\lambda$ stands for wavelength intervals; D_λ for relative spectrum distribution of illuminant D65; $v(\lambda)$ for spectral luminous efficiency for the field of view vision determining the average witness for spectrophotometric analysis; $\tau(\lambda)$ for spectral transmittance (%) and $\rho(\lambda)$ for spectral reflectance (%) are all included.

The following correlation yields the glass samples' visual absorbance in the visible zone.

$$A_{VIS} = 100 - T_{VIS} - R_{VIS}$$

Table 3.4 provided specifics on the information gathered from the UV-VIS spectrophotometer. The above visible properties can be used to determine how much natural light enters the buildings.

Table 3.3. FTIR band assignments on the spectra of tint glass based on (0.2Cu_2O-.07CuO-.03Fe_2O_3-0.3SnO_2)-0.4P_2O_5-30Na_2O-69SiO_2)(Fig. 3.4).

Points	Wave number (cm^{-1})	Functional Groups
a	**455**	**v_4 (O-Si-O) bending vibration and specific vibration of Fe-O bond**
b	**765**	**v Si-O (in SiO_4 tetrahedron)**
c	**1048**	**v_3 (Si-O) asymmetric stretching**
d	**1632**	**δ -H-O-H**
e	**3454**	**reticular v-OH**

3.3.3.2 *Solar Optical Properties*

Applying British and ISO standards, the solar optical characteristics of glass samples in the solar spectrum wavelength range of 360 nm to 830 nm are computed using the following formulas [71].

$$T_{solar} = \frac{\sum_{\lambda=360nm}^{\lambda=830nm} S_\lambda \tau(\lambda)\Delta\lambda}{\sum_{\lambda=360nm}^{\lambda=830nm} S_\lambda \Delta\lambda}$$

$$R_{solar} = \frac{\sum_{\lambda=360nm}^{\lambda=830nm} S_\lambda \rho(\lambda)\Delta\lambda}{\sum_{\lambda=360nm}^{\lambda=830nm} S_\lambda \Delta\lambda}$$

wherein S_λ represents the solar radiation's relative spectral distribution (W/m^2). The following correlation determines solar absorption.

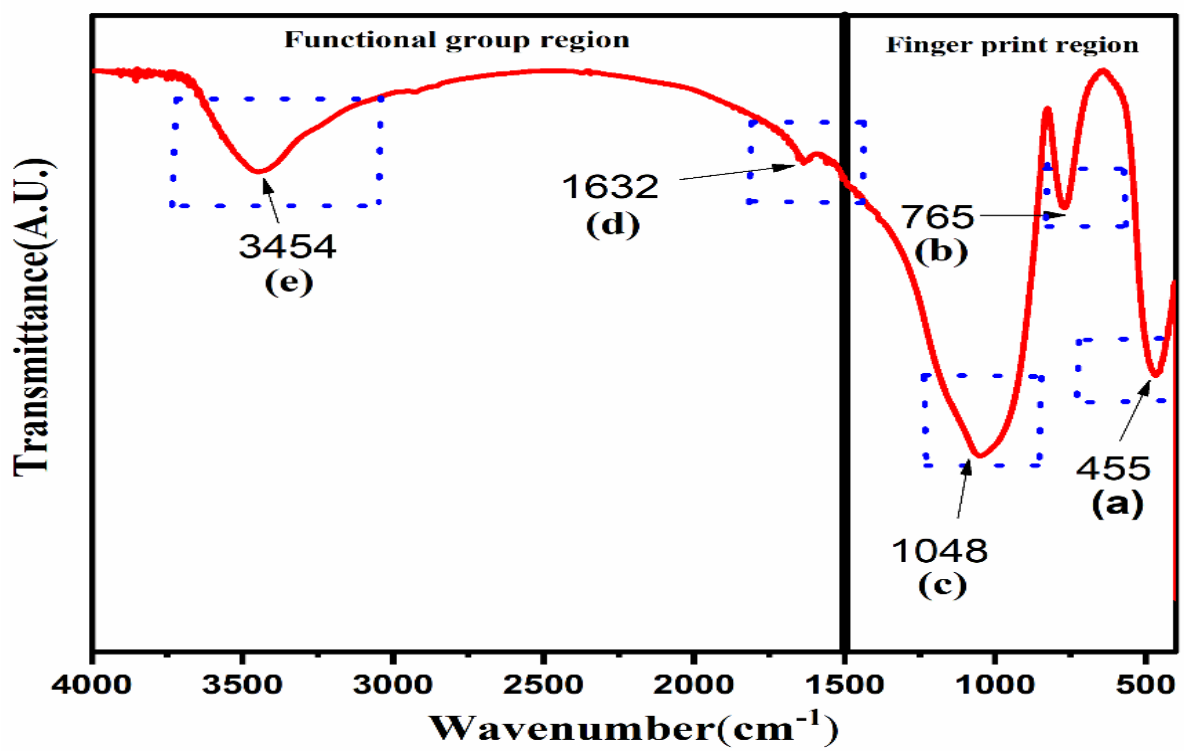

Fig.3.4 . The figure shows the infrared transmission spectra of tinted glass powder with compositions of $0.2Cu_2O$-.07CuO-.$03Fe_2O_3$-$0.3SnO_2$)-$0.4P_2O_5$-$30Na_2O$-$69SiO_2$.

$$A_{solar} = 100 - T_{solar} - R_{solar}$$

Building energy consumption rises due to the effects of solar optical characteristics on heating and cooling loads. These characteristics, indicated in **Table 3.4**, help determine how much heat enters buildings through glass windows.

3.3.3.3 *Refractive index (n) and extinction coefficient (k)*

According to Fresnel's theory, the refractive index (n), which is connected to the extinction coefficient (k) and the reflection function (R), is the real component of the complex refractive coefficient. The equation for this relationship is as follows.

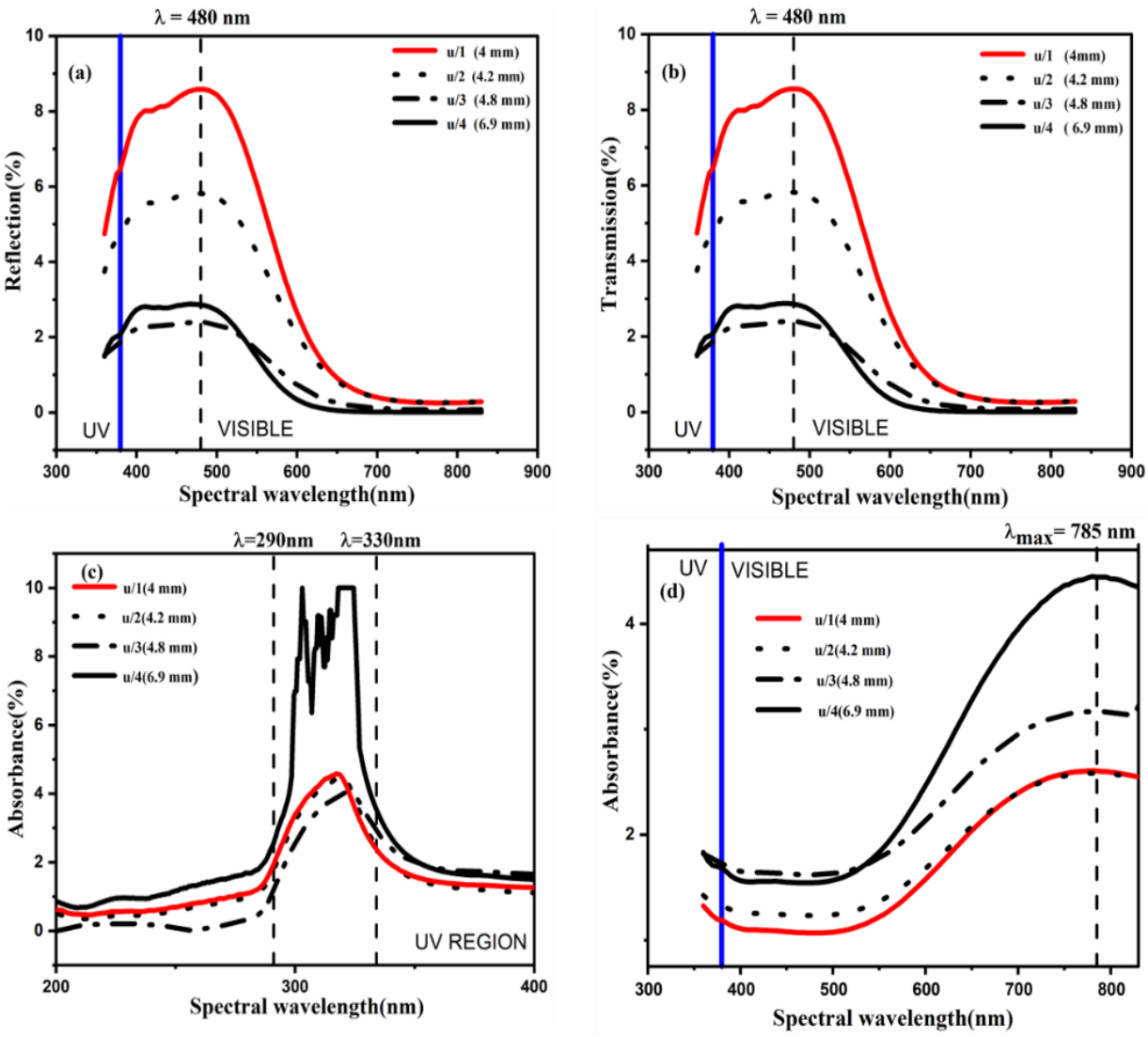

Fig. 3.5. (a) Tinted glass samples' spectral reflection in the visible and ultraviolet ranges. (b) Tinted glass samples' spectral transmission in the visible and ultraviolet spectrum. (c) The UV spectrum absorbance of tinted glass samples. (d) Tinted glass samples' spectral absorption in the visible and ultraviolet spectrums.

$$R = \frac{(n-1)^2 + k^2}{(n+1)^2 + k^2}$$

The following formulae are used to compute the refractive indices:

$$T_S = 10^{-A} \times 100$$

$$n = \frac{1}{T_s} + \sqrt{\frac{1}{(T_s - 1)}}$$

A represents absorbance and T_s is the percent transmittance constant or the percent transmittance. The following equation is used to compute the extinction coefficient (k).

Table 3.4. The table lists the optical characteristics of a few chosen synthesized tint glass samples.

Sample	Visible optical properties			Solar optical properties			E_{gind} (eV)	E_{gd} (eV)	E_U (eV)
	T_{VIS} (%)	R_{VIS} (%)	A_{VIS} (%)	T_{solar} (%)	R_{solar} (%)	A_{solar} (%)			
u/1	**44.62**	**44.45**	**10.93**	**39.18**	**39.04**	**21.79**	**3.52**	**3.68**	**.2976**
u/2	**42.00**	**41.00**	**17.00**	**35.00**	**35.00**	**30.00**	**3.54**	**3.71**	**.2941**
u/3	**30.73**	**30.77**	**38.50**	**21.78**	**21.79**	**56.43**	**3.50**	**3.63**	**.3584**
u/4	**28.00**	**28.00**	**44.00**	**18.00**	**18.00**	**64.00**	**3.51**	**3.72**	**.2985**

$$k = \frac{\alpha\lambda}{4\pi}$$

In which λ denotes the wavelength & α indicates the absorption coefficient of the material.

Two dominant transmission variables for the glass system's refractive index result are bridging and non-bridging anions and cations in the ultraviolet area and lattice vibrations in the glass networks in the infrared region [8]. Figs. 3.6 and 3.7 display the extinction coefficient and refractive index dispersion curves for each of the four tint glass samples, respectively. Yet, it has been shown that as the visible region's light wavelength increases, so do the refractive index and extinction coefficient of every glass sample, regardless of thickness.

3.3.3.4 ***Complex dielectric constant***

The refractive index (n) and extinction coefficient (k) determine the optical complex dielectric constant, which depends on the molecular mechanisms resulting from the interaction of light with electrons. The real and imaginary components of the complex dielectric constants are represented by $\mathcal{E}1$ and $\mathcal{E}2$, respectively. $\mathcal{E}1=n^2+k^2$ is the real part, and $\mathcal{E}2=2nk$ is the imaginary part [8]. **Fig. 3.8** displays the dispersion curves for the real and imaginary parts of the complex dielectric constant $\mathcal{E}1$ and $\mathcal{E}2$, respectively. In the visible region, both parts of the complex dielectric constant-real and imaginary-increase noticeably with wavelength for all glass samples of varying thicknesses.

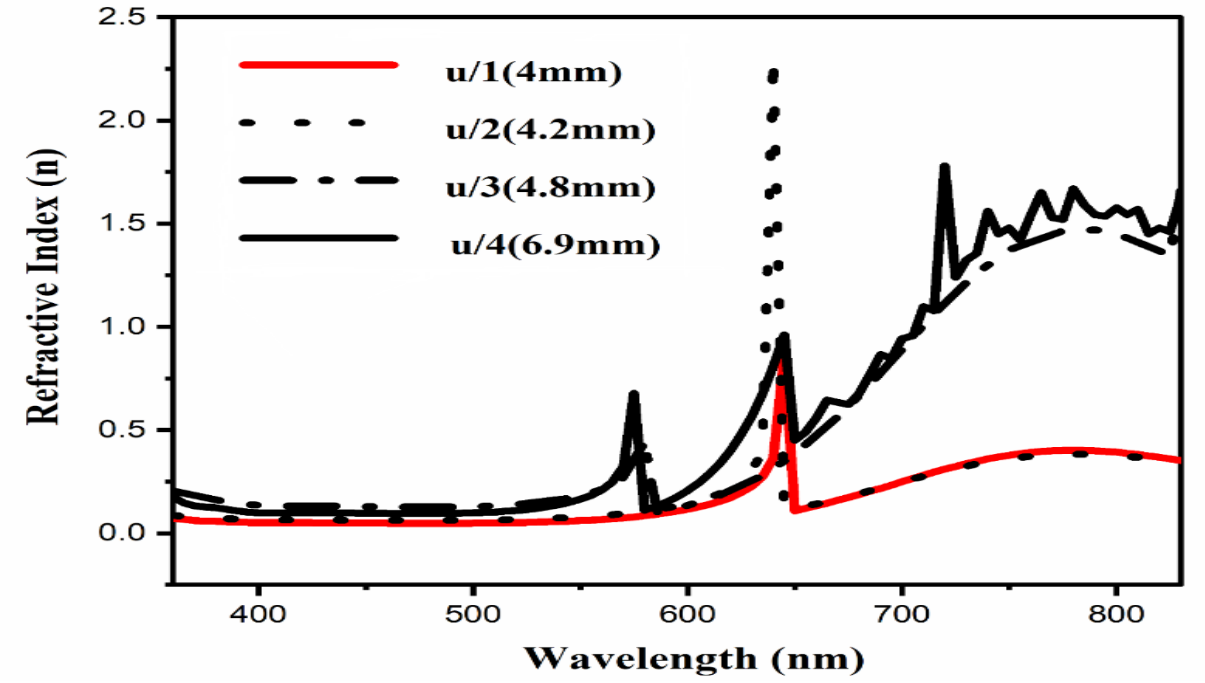

Fig. 3.6. Refractive index (n) dispersion curve with wavelength for tinted glass samples of varying thicknesses.

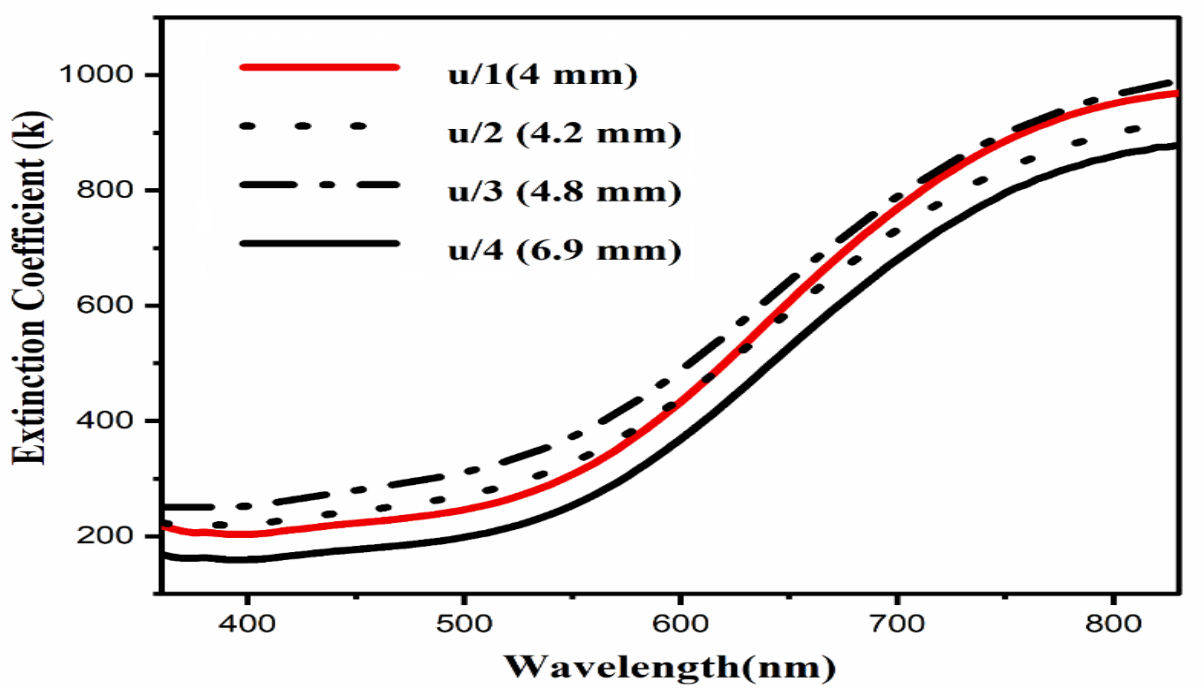

Fig. 3.7. Extinction coefficient (k) dispersion curve with wavelength for tinted glass samples of varying thicknesses.

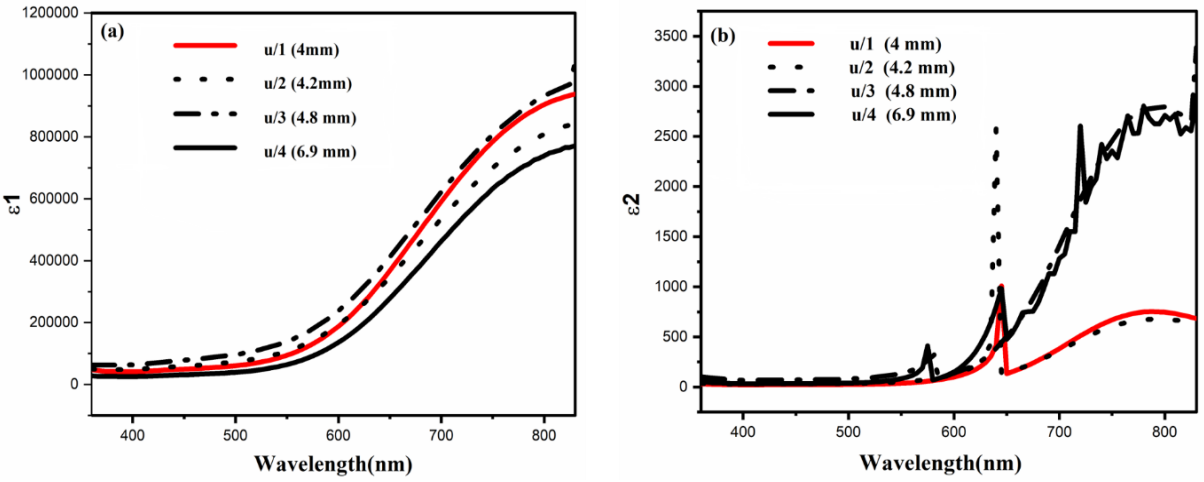

Fig. 3.8. (a) Dispersion curve of the real part of the complex dielectric constant ($\mathcal{E}1$) as a function of the wavelength for tint glass samples with varying thicknesses. (b) Dispersion curve of the imaginary part of the complex dielectric constant ($\mathcal{E}2$) as a function of the wavelength for tint glass samples with varying thicknesses.

3.3.3.5 *Assessment of the optical energy gap*

Tauc's plot of four identical optically polished samples with varying thicknesses for the direct and indirect transitions is displayed in **Fig. 3.9**. The following Davis and Mott formula is used to assess the energy gap of the samples made [**8**, **9**].

$$(\alpha hv) = B\left(hv - E_g\right)^r$$

In which r is the index number, which depends on the electronic transition route and has values of 1/2, 2, 3/2, and 1/3, and B represents the constant, E_g denotes the optical energy gap, and h indicates the plank constant. Generally, the r values for permitted electronic transitions are taken to be 2 for indirect transitions and ½ for direct transitions. The Tauc's plot between $(\alpha hv)^{1/r}$ on the vertical axis and photon energy (hv) on the horizontal axis is used to assess the optical band gap for each of the four samples with varying thicknesses. The optical band gaps are calculated from the linear part of the Tauc's plot sloped at $(\alpha hv)^r = 0$ (in which r=0.5 for indirect transition and r=2 for direct transition). **Table 3.4** lists the optical energy gap values for each of the four tint glass samples with varying thicknesses. It is noted that the determined metallic concentration (**Table 3.1**) in the glass matrix results in very modest direct and indirect optical energy gaps.

3.3.3.6 ***An assessment of Urbach energy***

Urbach energy is a measure of energetic disorder in an insulator or semiconductor's band edges. Localized states that are stretched in the band gap and formed as band tails in the usual band gap are present in low crystalline, poor crystalline, and disordered amorphous materials. The Urbach empirical rule describes the absorption coefficient (α) as a function of photon energy (hv) in the low photon energy band. The Urbach empirical rule equation is shown below.

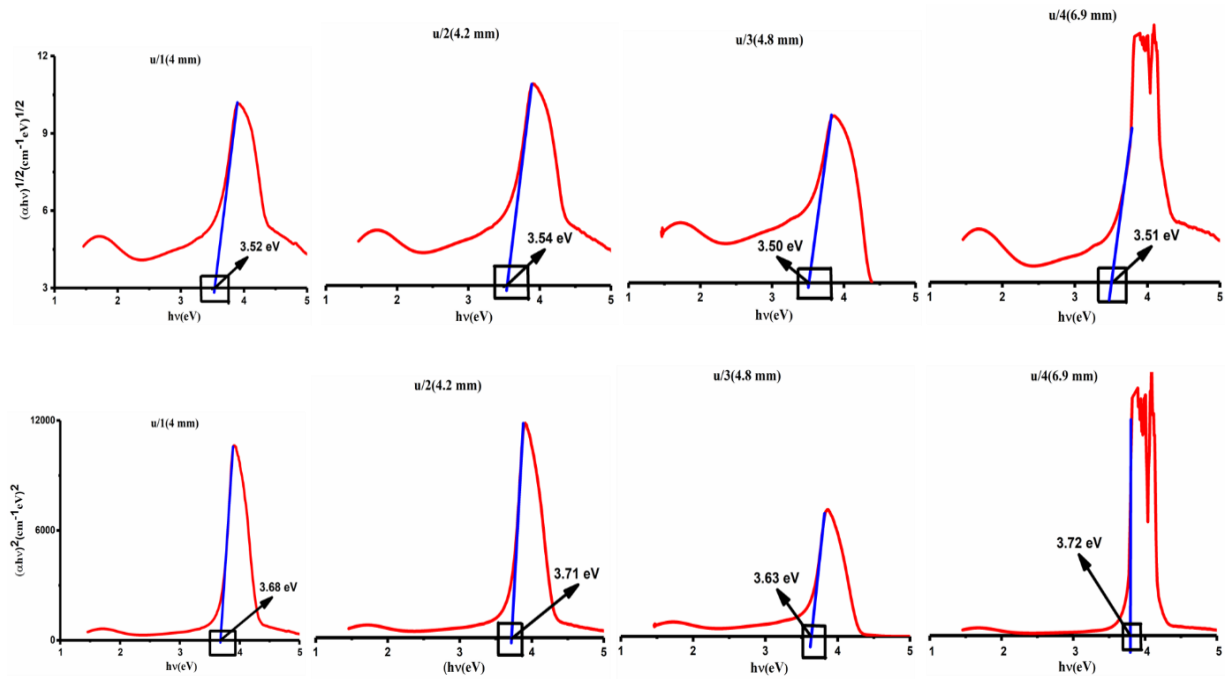

Fig. 3.9. The figure displays the Tauc plot for selected tinted glass samples of varying thicknesses, showing both direct and indirect transitions [8, 9].

$$\alpha = \alpha_0 \exp\left(\frac{hv}{E_U}\right)$$

Where E_U represents the band tail energy, also known as the Urbach energy, and α_0 acts as a constant.

Temperature has a negligible effect on Urbach energy. By taking the logarithms of the Urbach empirical rule equation on both sides, we obtain

$$\ln(\alpha) = \ln(\alpha_0) + \left(\frac{hv}{E_U}\right)$$

Plotting lnα versus the incident photon energy (hv) yields a straight line with m as its slope, hence Urbach energy $E_U = \frac{1}{m}$. Plotting $\ln(\alpha)$ versus incident photon energy (hv) for tint glass samples of varying thicknesses permits researchers to determine each sample's Urbach energy (**Fig. 3.10**). The disorder in the produced glass structures is reflected in the Urbach energy values of the four tint glass samples with varying thicknesses, which are listed in **Table 3.4**.

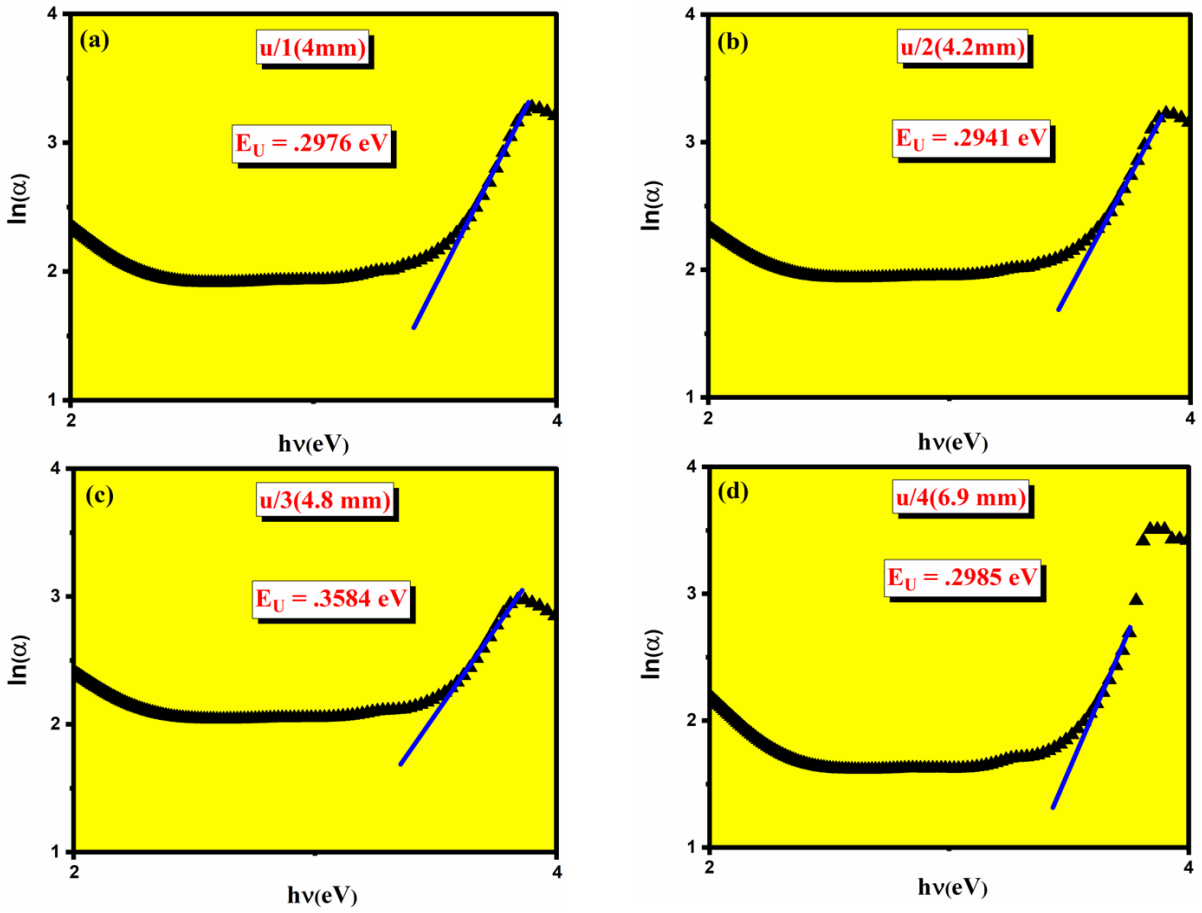

Fig. 3.10. The figure shows the plot of ln(α) versus the incident photon energy (hν) for tinted glass samples with varying thicknesses.

3.3.3.7 *Analysis of UV Absorption Edges*

In contrast to background losses (reflection loss, absorbance produced by OH groups, IR edge, etc.) observed in the absorbance spectra of iron, other dopants, refining agents, and absorbing contaminants, it is generally observed that the absorbance spectra of synthesized glass samples are primarily influenced by the host glass composition, melting temperature and time, oxygen partial pressure during melting and annealing temperature, and rate of cooling [72]. According to the resulting absorption analysis, the glass structure in question has a maximum absorbance of around 785 nm (λ_{max}) in the visible zone (**Fig. 3.5(d)**) and between 290 and 330 nm in the ultraviolet region (**Fig. 3.5(c)**). Under ordinary melting circumstances, the metallic component copper can

be found in the current-produced glass as Cu^{2+} ions, albeit part of it also remains as Cu^{0} and Cu_2O [**73** – **79**]. The Cu^{2+} ion gives a blue-to-green color which is dependent on the composition of the base glass, while the Cu^{+} ion has no visible absorption because of its $3d^{10}$ electronic configuration [**13**,**14**]. The cupric ion acts as a D-state ion having a $3d^{9}$ structure. Previous researchers discovered that the absorption band caused by the Cu^{2+} ion was detected at approximately 786 nm in silicate glasses, 1048 nm in alumina-boro-phosphate glasses, and 1390 nm in sodium alumina-borate glasses [**15**,**74**,**79**,**80**,**81**]. The current synthetic glasses exhibit a single broad absorption band that increases from 650 nm to a maximum absorbance of around 785 nm to 800 nm (**Fig. 3.5(d)**). This is most likely caused by the electronic transition of the cupric ions that are present in the ingredient. The electronic shift from the $^{2}\mathbf{E_g}$ to the $^{2}\mathbf{T_g}$ energy level in the octahedral coordination of the Cu^{2+} ion may be the cause of this expanding band, which suggests a distorted octahedral symmetry for the cupric ion in the current glass system [**81**,**82**]. Irons are an essential colorant in optical glasses and are one of the constituents in the current glass system. Although irons can exist in several oxidation states, they are primarily found in silicate glasses as Fe^{2+} and/or Fe^{3+} forms [**83**]. The chemistry of the glass matrix in which iron is contained, together with its redox and environment, are closely linked and can significantly affect the ensuing optical properties, including UV regulation [**84**,**85**]. In the current glass system, most of the iron is in the ferric Fe^{3+} form, as previous authors showed in many commercial oxide glasses with iron concentrations below <1%, which is comparable to iron concentration (**Table 3.1**) in the present glass system [**83**]. It is generally accepted that tetrahedral and octahedral Fe^{3+}ions can coexist in different silicate glasses, with the majority of Fe^{3+}ions being tetrahedral [**84**,**86-96**]. Ferric iron possesses a $3d^{5}$ electronic structure, while tetrahedral Fe^{3+} ions exhibit an absorption band in the visible region (645-769 nm) attributed to its first excited state to the ground state **($^{4}T_1(G)$**

→ $^{6}A_1(S)$) [87]. All Fe^{3+} d-d transitions result in a weak spin-forbidden absorption band because all Fe^{3+} d-d absorptions are spin-forbidden. The $^{4}T_1(G)$) → $^{6}A_1(S)$ transition of Fe^{3+}ions occurs in a spectral region, which may have been caused by a highly increasing absorption band above 650 nm in the absorption spectrum of produced entire glass samples (**Fig. 3.5(d)**) [84]. Due to the majority of Fe^{3+} transitions featuring the energy levels $^{4}E(D)$ → $^{4}T_2(D)$ and $^{4}A_1$, $^{4}E(G)$ happening in silicate glasses at wavenumbers within 500 and 370 nm, which overlap one another and are largely field-independent, it is also tough to distinguish the contributions of tetrahedral and octahedral Fe^{3+} sites. This may also have happened because of an increased absorption band seen from 500 nm to 290 nm in the visible and UV regions of the absorption spectrum of glass samples (Figs. 5(c) and 5(d)) [97]. Because of equipment constraints, it is not able to identify the spin-allowed $^{5}T_2(D)$ → $^{5}E(D)$ transition of Fe^{2+} ions occupying distorted octahedral sites, which is responsible for the absorption cantered at 1000 nm [84,85,97]. The possibility of an absorption band caused by the ligand in the metal charge assigning transition of Sn^{4+} cation, which is also present very little in the synthesized glass samples, may also be suggested by increasing the absorption band of the samples from 500 nm to 290 nm. These absorption bands were centered around 445 nm (visible region) [98].

3.3.4 *Physical and Mechanical Properties of Pigmented Glass*

The prepared glass material's extremely compact structure and low porosity are indicated by the minuscule difference between its soaking and dry weights (**Table 3.2**). The compressive stress-strain curves of three synthetic colored glass samples (A/1, A/2, and A/3) of varying thicknesses are shown in **Fig. 3.11**. The curves do not exhibit any discernible plastic deformation, and the bars were broken up into pieces upon compression. **Table 3.5** displays the compressive fracture strengths and measured elastic strain of approximately 1.8% for the resulting-coloured glass bars.

The stress-strain curves (**Fig. 3.11**) also forecast the specimens' fracture behavior in compression tests. The linear character of the stress-strain curves indicates the materials' elasticity. Young moduli of elasticity equal to the tangent value (m = stress/strain) were calculated using the approximately linear stress-strain curve (**Fig. 3.11**) that passes through the origin. **Table 3.5** displays the calculated values (young modulus) derived from stress-strain curves. Using the integration tool in Origin software at constant y baseline, the area under the stress-strain curves was also calculated to quantify the samples' modulus of toughness (energy absorbed per unit volume before fracture, measured in Joules.meter^{-3}). However, **Table 3.5** lists the expected compressive toughness moduli. The concentration of metallic components in the glasses is found to significantly increase their young modulus and compressive strength. The young modulus is approximately 146 compared to the regular glass young modulus of 70 GPa, and the compressive strength significantly improves from 1 GPa (the standard glass compressive strength) to about 3 GPa.

3.3.5 *Chemical Durability*

In **Table 3.6**, the chemical durability of the newly synthesized tint glass samples is shown as a weight loss (gram) and a parameter with dimensions (gram/cm^2.hour). According to the findings, the glass resists corrosive liquids quite well and loses very little weight.

3.4 Conclusions

According to this study, very low concentrations of iron oxide, tin oxide, copper, cupric oxide, and ammonium dihydrogen orthophosphate not only create a high-quality metallic tint glass system that significantly lowers the amount of solar heat energy that passes through it but also greatly

increase its compressive strength and young modulus. The new synthetic tint glass exhibits good chemical durability, lowers air conditioning loads, and lowers the cost of artificial daylighting in buildings. It can be produced at a very low cost because very little metallic concentration is needed to create the tint, which has a 28–44% visible transmittance (T_{VIS}) (**Table 3.4**) for daylighting and an 18–39% solar transmittance (T_{solar}) for heat gain into the building through the tinted glass with thicknesses ranging from 4–7 mm. The total amount of visible and solar transmission is quite like the total amount of visible reflection (R_{VIS}) and solar reflection (R_{solar}) of this prepared tinted glass. However, this kind of synthetic tint glass with the same variable thickness exhibits 21–64% solar absorbance (A_{solar}), which increases the amount of heat that enters the structure, and 10–44% visible absorbance (A_{VIS}), which decreases light visibility. Phosphorus silicate tint glass samples with the determined metallic content (**Table 3.1**) are successfully produced using the melt annealing process. The amorphous nature of the initial glass batch composition, the melted glass, and the powdered synthesized glass samples following heat treatment are all confirmed by X-ray diffraction tests. The synthesized optical polished rectangular tint glass samples' visible optical properties, solar optical properties, refractive index (n), extinction coefficient (k), optical energy gap (direct and indirect), and Urbach energy (E_U) were all calculated using the transmittance, reflectance, and absorbance data obtained by UV-Visible spectroscopy. In the 3.5–3.54 eV region, the indirect optical band gap (E_{gind}) is detected. The Urbach energy (E_U) is found between .2941 and .3584 eV, indicating that the glass system has an energetic disorder due to the concentration of metals. Mechanical parameters assessed by the ultimate tensile machine (UTM), such as compressive strength, young modulus, and module of toughness ($Kj.m^{-3}$), are improved by the identified metallic concentrations in the glass matrix. Compressive strength (σ_C), Young modulus (E), and toughness module ($Kj.m^{-3}$) of the glass samples with measured metallic

concentrations with changing thicknesses in the range of 12.07-12.88 mm (**Table 3.2**) values 2.92-2.98 GPa, 159-177 GPa, and 23360-26820 Kj.m^{-3}, respectively. While mechanical qualities are improved by increasing metallic concentrations, optical properties like as transparency are greatly diminished, resulting in undesirable black opaque glasses. Therefore, the goal of this research paper is to determine the ideal concentration of metallic ingredients in phosphorus silicate glass systems that result in high-quality blue optical glasses with significant mechanical qualities and transparency that could be very helpful as building materials in the not-too-distant future.

Table 3.6. Chemical resistance of selected tint glass samples.

Sample	**Surface area(cm^2)**	**Weight loss(gram) $(W_i - W_f)$**	**Chemical durability (gram / (cm^2.hour) $(\frac{W_i - W_f}{st})$**	**Corrosive liquid**
A/1	**5.6**	**0**	**0**	**HNO_3**
A/4	**21.5**	**0**	**0**	**H_2SO_4**
A/6	**23.6**	**.1126**	**2.83×10^{-5}**	**HCl**

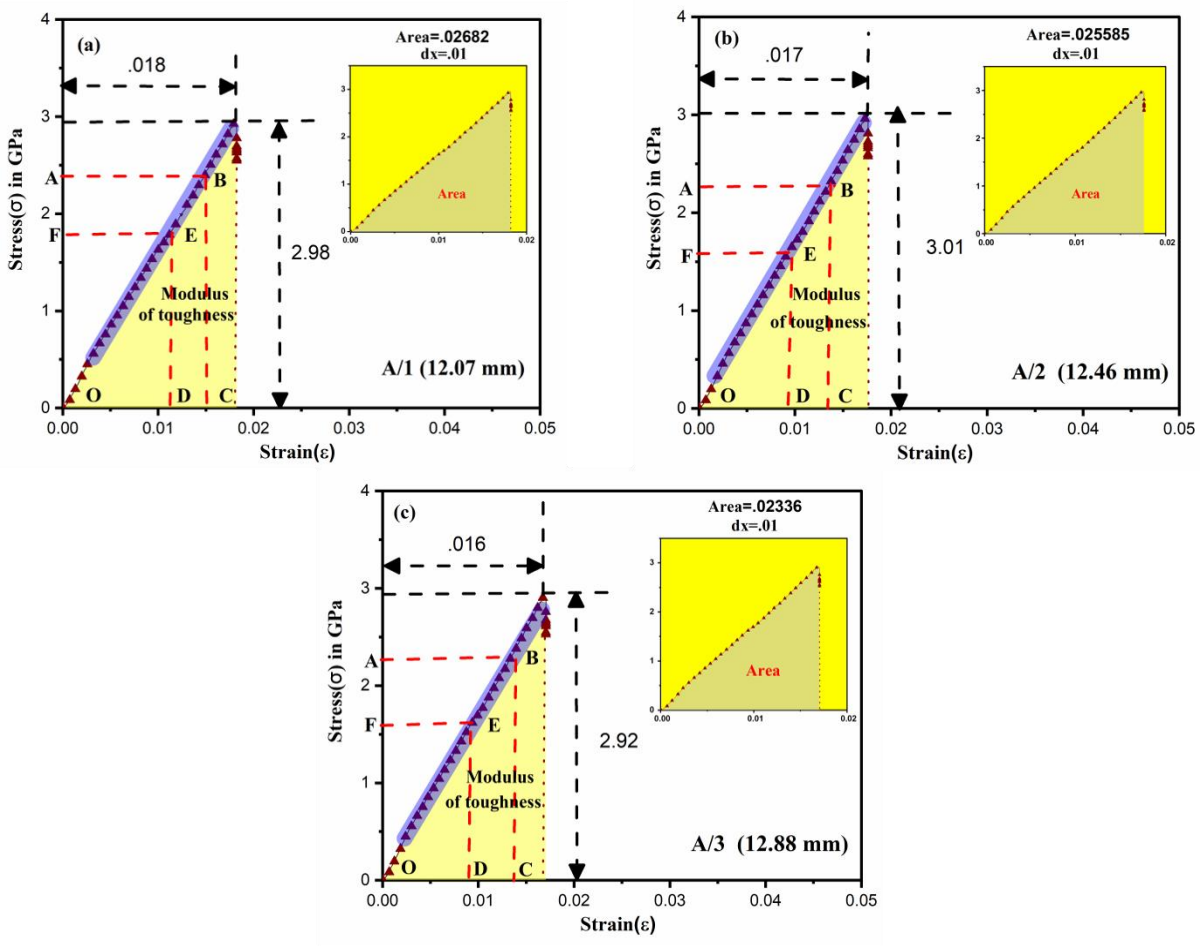

Fig. 3.11. Stress-strain curves of selected tint glass samples, with Young's Modulus and toughness derived from these curves.

Table 3.5. Mechanical characteristics of the chosen synthesized tint glass samples.

Sample	σ_C(GPa)	E (GPa)	Module of toughness(Kj.m^{-3})
A/1	2.98	159.11	26820
A/2	3.01	169.89	25585
A/3	2.92	176.86	23360